Composites Part B 132 (2018) 237–243

Contents lists available at ScienceDirect

Composites Part B

journal homepage: www.elsevier.com/locate/compositesb

Investigations for mechanical properties of Hap, PVC and PP based 3D porous structures obtained through biocompatible FDM filaments

Ravinder Sharma [a], Rupinder Singh [a], R. Penna [b], F. Fraternali [b, *]

[a] Production Engineering, Guru Nanak Dev Engineering College, Ludhiana, India
[b] Civil Engineering, University of Salerno, Italy

ARTICLE INFO

Article history:
Received 19 June 2017
Accepted 28 August 2017
Available online 9 September 2017

Keywords:
Fused deposition modelling
Hap
PVC
PP
Tensile testing

ABSTRACT

In last two decades fused deposition modelling (FDM) has emerged as a standout amongst the most broadly utilized process for fabrication of 3D functional parts in bone tissue engineering. However this technique is still facing substantial problems to produce porous structure having sufficient mechanical strength. In this present research an exertion has been made to develop a bio-compatible FDM filament which has been further used to fabricate 3D porous structure. The results of the study highlighted the effect of FDM process parameters (infill percentage, infill speed and layer thickness) on the tensile properties (percentage elongation at peak, percentage elongation at break and yield stress) of the 3D functional prototypes. It has been observed that infill percentage has major contribution i.e. 92% towards peak elongation, 91% towards break elongation and 80% towards yield stress. The remaining two parameters have very less contribution towards mechanical properties of the 3D structures. For microscopic analysis the microphotographs of scanning electron microscope (SEM) have been taken to ensure the structure produced is porous enough and can be used in a variety of engineering and biomedical applications.

1. Introduction

The additive manufacturing (AM) processes has an imperative role in the realm of bone tissue engineering (BTE). The traditional implant fabrication processes has become obsolete with the advancement in various AM techniques. All AM processes work on the same principal of successive addition of layers to fabricate a final product [1]. The AM acts as a backbone in the bio-manufacturing sector. Recently AM has been successively used to produce the complex 3D tailor made bio-structures [2]. BTE used to replace or restore the physiological functions that have been lost in the damaged or diseased organs [3]. Tissue engineering (TE) involves the combinations of cells and biomaterials for assembly of tissue structures [4]. In BTE the "top-down" approach (see Fig. 1) is used. In this approach, on the scaffolds with biodegradable and biocompatible properties cells are seeded [5–7]. The population of cells is directly proportional to the spacing in the scaffold, but the fabrication of complex functional porous scaffolds using conventional methods still confronts challenges [8–10].

The AM processes has been used to produce the open porous scaffolds of biomaterials for providing the mechanical support to the cells and significant space for the regeneration of tissue [12]. The AM processes produces the sacrificial patterns for casting of patient specific best fit functional implants [13]. According to type of raw material used for building processes the current AM can be broadly categorized into four classes powder form, gas phase, sheet form and liquid phase [14,15]. These techniques are also classified on the basis of source of power used i.e. laser and heat. The laser based AM processes demands more considerations towards their care and maintenance and setups are also exorbitant in contrast to non-laser based methods [16]. FDM stands second after stereo-lithography as most commonly used AM technologies [17]. The fabrication of scaffolds starts from MRI or CT scanned data of implant and converted into 3D geometry by using software such as 3D-Doctor, MIMICS etc. and saved into STL (stereo-lithography or standard triangulation language) format, i.e. appropriately used by any AM techniques [18]. The STL file is sliced into two dimensional layers by using software support [19]. The commercial FDM printers accompanied a temperature controlled hot chamber [20]. The thermoplastic is extruded through the extrusion head on the

* Corresponding author.
E-mail addresses: rupindersingh78@yahoo.com (R. Singh), rpenna@unisa.it (R. Penna), f.fraternali@unisa.it (F. Fraternali).

http://dx.doi.org/10.1016/j.compositesb.2017.08.021
1359-8368/

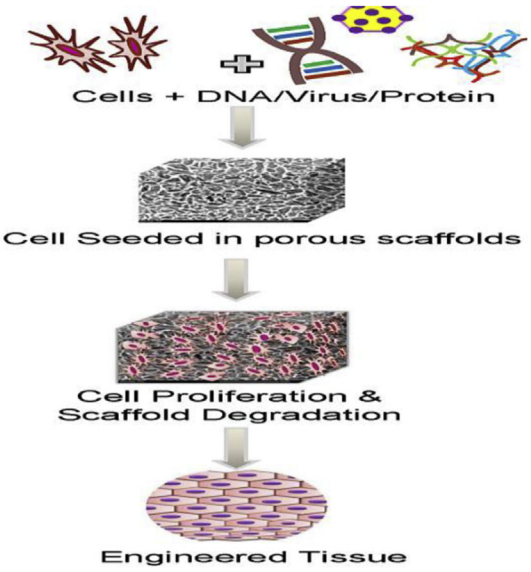

Fig. 1. Schematic of "top-down" approach for tissue engineering [11].

fixtureless platform [21]. To prevent solidified material from the thermal stresses the temperature of the chamber is maintained constant above the glass transition temperature i.e. 72 °C in case of ABS [22–25].

In this research an exertion has been made to develop a new ceramic based FDM filament for clinical dentistry. The biocompatible polymers has been used as base matrixes and reinforced with the bioactive ceramics. The 3D-porous structures have been fabricated by running this in house developed filament on existing FDM setup and further investigations have been made for mechanical properties. The obtained results have been supported by images obtained from the SEM.

2. Materials and methods

The experimentation work starts from the collection of biocompatible polymers PP and PVC in the granular form. The bioactive ceramic hydroxyapatite (Hap) has been reinforced in the parent polymer matrixes. A fixed proportion of Hap and the polymer matrix as 4%HAp+96%polymer matrix (PVC70% + PP30%) have been used for preparing a filament. Twin screw extruder was used for blending and extrusion of FDM filament. Fig. 2 shows in house extruded filament.

To fabricate the 3D structures for mechanical testing and SEM analysis a commercial FDM setup (3D printer, Make-Divide By Zero, India) has been used shown in Fig. 3.

Three different controllable parameters (i.e. layer thickness, infill percentage and infill speed) of FDM has been selected (see Table 1) based upon pilot study.

Whereas other remaining FDM process parameters such as orientation, raster angle, temperature etc. was put as constant throughout in the present research work. Extrusion temperature was set according to melting point of the parent matrix. The standard 3D structures fabricated on FDM (as per ASTM D-638 IV) have been mechanically tested on universal tensile tester (UTT). The complete control log as per Taguchi L9 orthogonal array is shown in Table 2.

A total 3 sets of repetitions/experiments have been performed for 9 settings of different controllable factors (as per Taguchi L9 OA). After performing the tensile testing, the part with best mechanical properties was used for microscopic analysis by taking the micro-photographs through SEM.

Fig. 2. In-house extruded FDM filament.

Fig. 3. FDM setup used for 3D printing.

Table 1
FDM input process parameters.

Levels	Parameters		
	Infill percentage %	Layer thickness mm	Infill speed mm/s
Level 1	0.20	0.25	33
Level 2	0.60	0.30	35
Level 3	1.0	0.35	37

Table 2
Control log and input parameters.

Exp. no.	Parameter(A) Infill percentage	Parameter(B) Layer thickness (mm)	Parameter(C) Deposition speed (mm/min)
1	20	0.25	33
2	20	0.30	35
3	20	0.35	37
4	60	0.25	35
5	60	0.30	37
6	60	0.35	33
7	100	0.25	37
8	100	0.30	33
9	100	0.35	35

Table 3
Observed values of mechanical testing.

Exp. no.	(A)	(B)	(C)	Peak elongation %	Break elongation %	Yield stress MPa
1	20	0.25	33	1.41	1.55	0.24
2	20	0.30	35	1.33	1.37	0.04
3	20	0.35	37	1.28	1.35	0.03
4	60	0.25	35	2.25	2.56	1.66
5	60	0.30	37	2.04	2.26	0.91
6	60	0.35	33	1.90	2.13	0.71
7	100	0.25	37	3.04	3.25	3.47
8	100	0.30	33	2.59	2.73	1.14
9	100	0.35	35	2.30	2.46	0.75

3. Results and discussion

3.1. Mechanical properties

After successful completion of pilot experimentation at pre-selected levels of process variables, 3D structures were fabricated on FDM for mechanical testing. The resulted values of percentage elongation at peak, percentage elongation at break and yield stress at the subjected input parameters are shown in Table 3.

The ANOVA has been used for “Larger the Better” type case. The universal tensile tester (Make: Shanta Engineering) has been used for mechanical testing of specimens using load cell 10 KN.

3.2. Elongation at peak

The literature reviews reveals that the infill percentage majorly affects the mechanical strength of the specimens [26,27]. If it increases from 20% to 100% then tensile strength of the prototype is raised by 250% [28]. The signal to noise ratio (S/N) graph for peak elongation values at larger the better type is shown in Fig. 4.

As observed from Fig. 4, as the infill percentage is increased from minimum (20%) to maximum (100%) density level the percentage elongation at peak of the parts increased. Maximum elongation is achieved in parts having density 100%. In case of layer thickness, published research papers suggested that the tensile strength of the parts has been decreased when layer thickness changes from 0.25 to 0.35 mm [29]. The S/N ratio shows that with the increase of layer thickness from 0.25 to 0.35, the peak elongation has been decreased it is decreased due to lesser number of layers with the increase of thickness and lesser contact between the layers which may lead to reduce the mechanical strength.

The infill speed does not possess much effect on the peak elongation as it varies around the mean value.

Analysis of variance of S/N ratio for elongation at peak shows that only one input parameter (see Table 4) has been found significant at 95% confidence level.

The S/N ratio at larger the better for elongation at peak is shown in Table 5. It has been found that the main effect on peak elongation is of infill density and very less effect of layer thickness and deposition speed.

To calculate the optimized value following equation has been used.

$$\eta_{opt} = m + (m_{A3} - m) + (m_{B1} - m) + (m_{C3} - m) \quad (1)$$

where ‘m’ is overall mean of S/N values that has been obtained from MINITAB, m_{A3} is the mean of S/N values for infill density at level 3 and $m_{B1}$and mc_3 are mean of S/N values for layer thickness and deposition speed at level 1 and level 3 respectively.

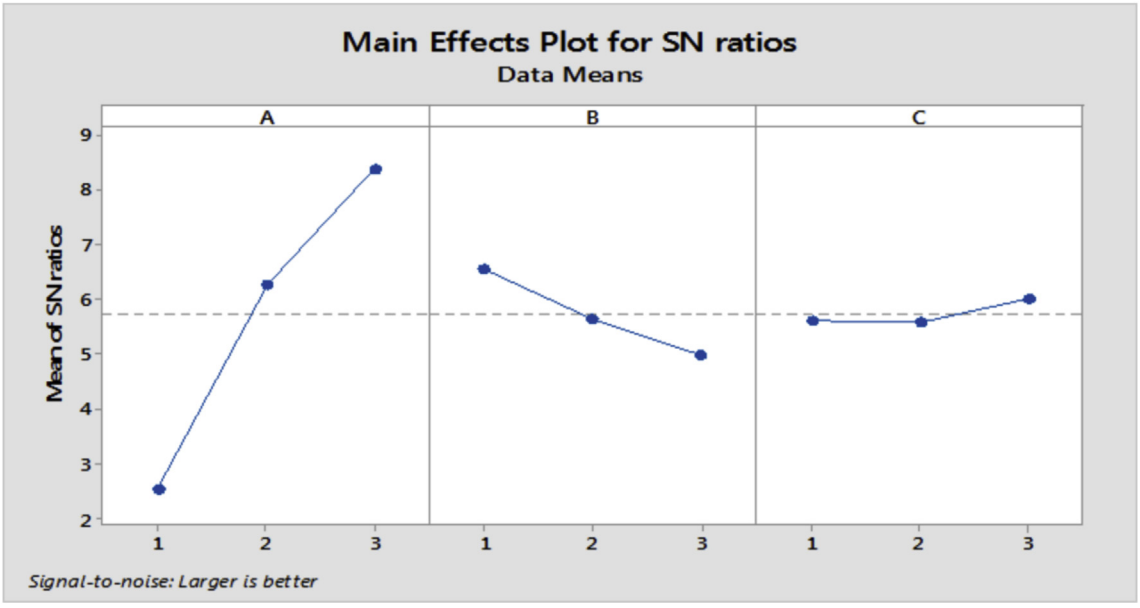

Fig. 4. S/N response to peak elongation data.

Table 4
Analysis of Variance for SN ratio for peak elongation.

Factor	DoF	SS	F	P	Percentage contribution
A	2	52.66	167.07	0.006	92.29%
B	2	3.76	11.94	0.077	6.59%
C	2	0.32	1.02	0.494	0.56%
Residual Error	2	0.32	–	–	0.56%
Total	8	57.06	–	–	100%

Table 5
Response table for S/N ratio (larger the better) for peak elongation.

Levels	A	B	C
1	2.535	6.562	5.608
2	6.270	5.645	5.585
3	8.386	4.985	5.998
Delta	5.851	1.577	0.413
Rank	1	2	3

$yopt2 = (1/10)^{\eta opt/10}$ for properties, lesser the better
$yopt2 = (10)\eta_{opt}/10$ for properties, largest the better
So.m = 5.73.

Now from the Table 5.

$m_{a3} = 8.38$, $m_{b1} = 6.56$ and $m_{c3} = 5.99$.
$\eta_{opt} = 5.73+(8.38-5.73)+(6.56-5.73)+(5.99-5.73)$.
Now $\eta_{opt} = 9.47$ dB
$y^2_{opt} = (10)^{\eta opt/10}$
$y_{opt2} = (10)^{9.47/10}$
$y_{opt} = 2.97$

The calculated value for % of elongation at peak was 2.97 which isnearest to the value observed for experiment no. 7 (see Table 3).

3.3. Elongation at break

The S/N ratio plot for elongation at break is shown in Fig. 5.
It suggests that with the increase of infill percentage from low density to high density the % elongation value increases and in case of layer thickness when it increases the % elongation has been decreased. This may be due to more spacing between the respective layers. The deposition speed does not show much effect on the break elongation as it lies near around the mean line. Table 3 shows that the parametric conditions at experiment number 7 was better for elongation at peak.

Table 6
Analysis of Variance for SN ratios (larger the better) for break elongation.

Factor	DoF	SS	F	P	Percentage contribution
A	2	55.34	321.26	0.003	91.03%
B	2	5.06	29.34	0.033	8.32%
C	2	0.22	1.23	0.449	0.37%
Residual Error	2	0.17			0.28%
Total	8	60.79			100%

Table 7
Response Table for ranking of input parameters (larger the better) for brake elongation.

Levels	A	B	C
1	3.049	7.448	6.366
2	7.316	6.180	6.284
3	8.927	5.664	6.642
Delta	5.877	1.784	0.358
Rank	1	2	3

Analysis of variance for S/N ratio at larger the better shows that two input parameters have significant effect on the break elongation. It has been observed at 95% confidence level that infill percentage and layer thickness affects more than 91% and 8% respectively on the elongation at break values (see Table 6).

Table 7 shows response for S/N ratio at larger is better type case, which suggests that the infill percentage has maximum contribution and deposition speed has minimum effect on break elongation.

The optimized value was calculated according equation (1).

Here m = 6.43

Fig. 5. S/N response to break elongation.

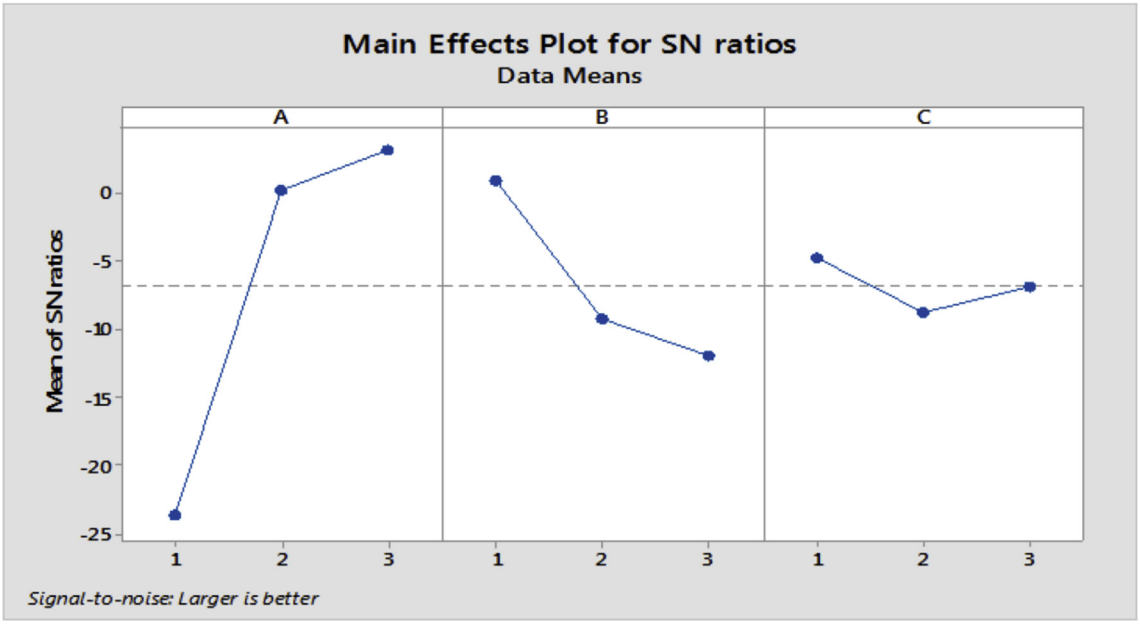

Fig. 6. S/N response to yield stress.

From Table 7,

$m_{A3} = 8.92, m_{B1} = 7.44$ and $m_{C3} = 6.64$.
$\eta_{opt} = 6.43+(8.92-6.43)+(7.44-6.43)+(6.64-6.43)$
Now $\eta_{opt} = 10.14$ dB
$y^2_{opt} = (10)^{\eta opt/10}$
$y_{opt2} = (10)^{10.14/10}$
$y_{opt} = 3.21$

The calculated value for break elongation was 3.21 which isnearest to the value observed for experiment no. 7 (see Table 3).

3.4. Yield stress

The S/N ratio plot for the yield stress is shown in Fig. 6.

S-N graph suggests that yield stress of the material is directly proportional to the infill percentage. Hence with the increase of infill density from lower to higher level the yield stress of the material has been raised. But in case of layer thickness yield stress is inversely proportional to the thickness of layer. So with the increase of layer thickness yield stress has been decreased. Infill speed does not put much effect on the yield strength but maximum yield stress is obtained at minimum deposition speed. The analysis of variance for S/N ratio at larger the better is shown in Table 8.

It suggests that there are two input parameters that have significant effect on the yield stress. It has been observed at 95% confidence level that infill percentage affects more than 80% on the yield stress. Whereas effect of layer thickness also more than 17% on the yield strength.

Table 9 shows response for S/N ratio at larger is better type case, which suggests that the infill percentage has maximum contribution and deposition speed has minimum effect on yield stress.

The optimized value was calculated according equation (1).

from Minitab $m = -6.75$

Now from Table 9,

$m_{A3} = 3.15, m_{B1} = 0.93$ and $m_{C3} = -4.74$.
$\eta_{opt} = -6.75+(3.15 + 6.75)+(0.93 + 6.75)+(-4.74 + 6.75)$
Now $\eta_{opt} = 12.84$ dB
$y^2_{opt} = (10)^{\eta opt/10}$
$y_{opt2} = (10)^{42.18/10}$
$y_{opt} = 4.38$

The calculated value for yield stress was 4.38 which is very close to the experiment performed at the optimum observed parameters of FDM and observed value is 4.24.

3.5. Microscopic analysis

After successful runs of mechanical testing, the specimen showing better mechanical properties has been used for microscopic analysis. The microphotographs of the specimen have been taken with the help of JEOL JSM-6510LV SEM (Japan). Avery thin layer of gold has been coated on the samples to get good conductivity. The SEM was conducted on the fractured surfaces of the samples prepared by tensile testing. The microphotographs suggest

Table 8
Analysis of Variance for SN ratios (larger the better) for yield stress.

Factor	DoF	SS	Adj SS	Mean of SS	%
A	2	1291	1291	645.5	80.39
B	2	277	277	138.7	17.27
C	2	23	23.	11.5	1.45
Residual Error	2	14	14.	7	0.88
Total	8	1605			

Table 9
Response Table for ranking of input parameters (larger the better) for yield stress.

Levels	A	B	C
1	−23.60	0.93	−4.74
2	0.20	−9.21	−8.69
3	3.15	−11.98	−6.82
Delta	26.75	12.91	3.94
Rank	1	2	3

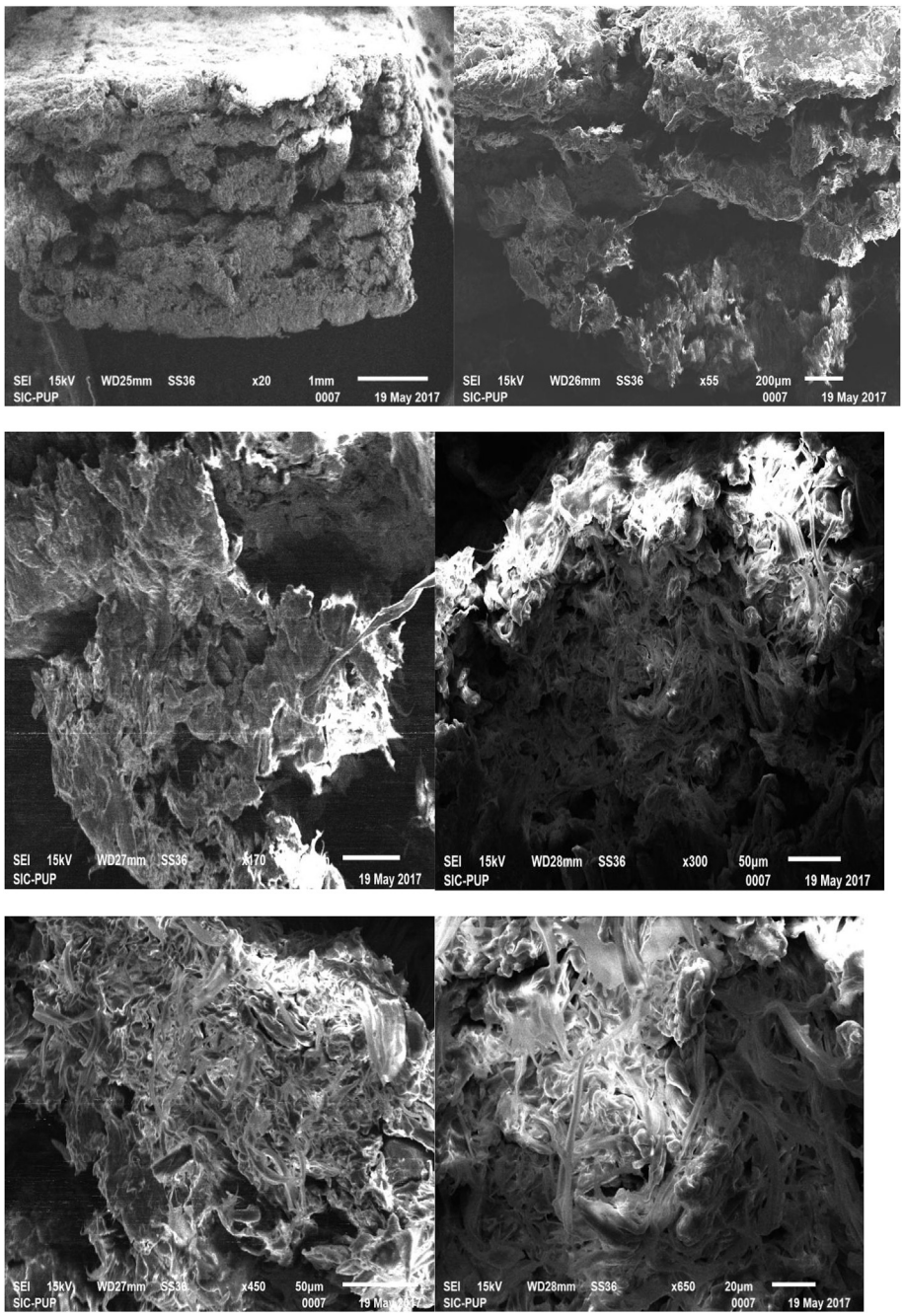

Fig. 7. Microphotographs of the specimen taken on SEM.

that the fabricated parts are having uniformly open, porous and fibrous structure (see Fig. 7) which are sufficiently good for growth of cells and are suitable in clinical dentistry.

4. Conclusions

The 3D porous structures have been fabricated through FDM and observed with SEM. Following are the conclusions of this study.

- The standard 3D prototypes (as per ASTM D-638) have been fabricated on FDM. It has been observed that when the infill percentage has been increased from low density to medium density level and further towards the solid, percentage of elongation at peak of the specimen has been increased from 1.28 (specimen no. 3) to 3.04 (specimen no. 7). The elongation at break is also increased with the change in density from low to high. The outcomes are in accordance with the perceptions made by different investigators [28].
- The effect of layer thickness has been also investigated. The best value of peak elongation, break elongation and yield stress have been obtained at minimum value of layer thickness i.e.0.25 mm. When the layer thickness was increased from 0.25 to 0.30 and 0.35 the percentage elongation in both cases has been decreased. The value of yield stress has been also decreased by

increasing the layer thickness. In the present work the infill speed has not demonstrated huge impact on the mechanical properties of the specimen.

The microphotographs obtained from the SEM shows that the specimens fabricated by FDM are having open porous and fibrous structure, which increases the cell cultivation rate for regeneration of new tissues inside the body. Since the functional prototypes are having porous and fibrous structure, they can be successfully used in a variety of engineering applications and clinical dentistry.

We address studies on the use of recycled polymers for the manufacturing of the investigated FDM filaments [30], the mechanical modelling of their properties through micromechanical approaches and poroelasticity [31,32], and use of such materials for the fabrication of lightweight innovative metamaterials and structures [33–45] to future work.

Funding

The authors are highly thankful to University Grants Commission, Government of India, File. No. F.30-66/2016 (SA-II) for financial support.

References

[1] Singh S, Ramakrishna S, Singh R. Material issues in additive manufacturing: a review. J Manuf Process 2017;25:185–200.
[2] Widmer S, Mikos A. Fabrication of biodegradable polymer scaffolds for tissue engineering. Front tissue Eng 1998;20:107–20.
[3] Bhatia S, Chen C. Tissue engineering at the micro-scale. Biomed Microdevices 1999;2(2):131–44.
[4] Tsang V, Bhatia S. Three-dimensional tissue fabrication. Advanced drug delivery reviews 2004;56(11):1635–47.
[5] Lu T, Li Y, Chen T. Techniques for fabrication and construction of three-dimensional scaffolds for tissue engineering. Int J Nanomed 2013;8(2):337–50.
[6] Huang GY, Zhou LH, Zhang QC, Chen YM, Sun W. Microfluidic hydrogels for tissue engineering. Biofabrication 2011;3(1):012001.
[7] Korossis S, Bolland F, Southgate J, Ingham E, Fisher J. Regional biomechanical and histological characterisation of the passive porcine urinary bladder: implications for augmentation and tissue engineering strategies. Biomaterials 2009;30(2):266–75.
[8] Wimpenny I, Ashammakhi N, Yang Y. Chondrogenic potential of electrospunnanofibres for cartilage tissue engineering. J tissue Eng Regen Med 2012;6(7):536–49.
[9] Groeber F, Holeiter M, Hampel M, Hinderer S. Skin tissue engineering—in vivo and in vitro applications. Adv drug Deliv Rev 2011;63(4):352–66.
[10] Ingber D, Mooney D, Langer R. Tissue engineering by cell transplantation using degradable polymer substrates. J Biomech Eng 1991;13:143–51.
[11] Tiruvannamalai-Annamalai R, Armant DR, Matthew HWT. A glycosaminoglycan based, modular tissue scaffold system for rapid assembly of perfusable, high cell density, engineered tissues. PLoS One 2014;9(1):e84287. https://doi.org/10.1371/journal.pone.0084287.
[12] Wei G, Ma X. Nanostructured biomaterials for regeneration. Adv Funct Mater 2008;18(22):3568–82.
[13] Eggbeer D, Bibb R, Williams R. The computer-aided design and rapid prototyping fabrication of removable partial denture frameworks. Proc Instit Mech Eng Part H J Eng Med 2005;219(3):195–202.
[14] Leu MC, Zhang W. Research and development in rapid prototyping and tooling in the United States. In: Proc. of first international conference on rapid prototyping and manufacturing, Beijing, China; 1998.
[15] Liu Q, Sui G, Leu MC. Experimental study on the ice pattern fabrication for the investment casting by rapid freeze prototyping (RFP). Comput Ind 2002;48(3):181–97.
[16] Singh S, Singh R. Fused deposition modelling based rapid patterns for investment casting applications: a review. Rapid Prototyp J 2016;22(1):123–43.
[17] Jain P, Kuthe AM. Feasibility study of manufacturing using rapid prototyping: FDM approach. Procedia Eng 2013;6:4–11.
[18] Singh R, Singh S, Fraternali F. Development of in-house composite wire based feed stock filaments of fused deposition modelling for wear-resistant materials and structures. Compos Part B Eng 2016;98:244–59.
[19] Chua CK, Leong KF, Lim CS. Rapid prototyping: principles and applications. World Scientific; 2010.
[20] Sahebrao ID, Madhusudan KA, Thakare SB, Talankar AS. Rapid prototyping—a technology transfer approach for development of rapid tooling. Rapid Prototyp J 2009;15(4):280–90.
[21] Boschetto A, Giordano V, Veniali F. 3D roughness profile model in fused deposition modelling. Rapid Prototyp J 2013;19(4):240–52.
[22] Ivanova O, Williams C, Campbell T. Additive manufacturing (AM) and nanotechnology: promises and challenges. Rapid Prototyp J 2013;19(5):353–64.
[23] Wohlers T. Wohlersreport. Wohlers Associates, Inc; 2012.
[24] Garg H, Singh R. Investigations for melt flow index of Nylon6-Fe composite based hybrid FDM filament. Rapid Prototyp J 2016;22(2):338–43.
[25] Ning F, Cong W, Hu Y, Wang H. Additive manufacturing of carbon fiber-reinforced plastic composites using fused deposition modeling: effects of process parameters on tensile properties. J Compos Mater 2016;51(4):451–62.
[26] Singh R, Singh S. Development of nylon based FDM filament for rapid tooling application. J Instit Eng India Ser C 2014;95(2):103–8.
[27] Carneiro OS, Silva AF, Gomes R. Fused deposition modeling with polypropylene. Mater Des 2015;83:768–76.
[28] Ning F, Cong W, Qiu J, Wei J, Wang S. Additive manufacturing of carbon fiber reinforced thermoplastic composites using fused deposition modeling. Compos Part B Eng 2015;80:369–78.
[29] Onwubolu GC, Rayegani F. Characterization and optimization of mechanical properties of ABS parts manufactured by the fused deposition modelling process. Int J Manuf Eng 2014.
[30] Singh N, Hui D, Singh R, Ahuja IPS, Feo L, Fraternali F. Recycling of plastic solid waste: a state of art review and future applications. Compos Part B Eng 2017;115:409–22.
[31] Lucantonio A, Tomassetti G, De Simone A. Large-strain poroelastic plate theory for polymer gels with application to swelling-induced morphing of composite plates. Compos Part B Eng 2017;115:330–40.
[32] Khezrzadeh H. A statistical micromechanical multiscale method for determination of the mechanical properties of composites with periodic microstructure. Compos Part B Eng 2017;115:138–43.
[33] Naddeo F, Naddeo A, Cappetti N. Novel “load adaptive algorithm based” procedure for 3D printing of lattice-based components showing parametric curved micro-beams. Compos Part B Eng 2017;115:51–9.
[34] Fraternali F, Spadea S, Berardi VP. Effects of recycled PET fibers on the mechanical properties and seawater curing of Portland cement-based concretes. Constr Build Mater 2014;61:293–302.
[35] Farina I, Fabbrocino F, Carpentieri G, Modano M, Amendola A, Goodall R, et al. On the reinforcement of cement mortars through 3D printed polymeric and metallic fibers. Compos Part B Eng 2016;90:76–85.
[36] Farina I, Fabbrocino F, Colangelo F, Feo L, Fraternali F. Surface roughness effects on the reinforcement of cement mortars through 3D printed metallic fibers. Compos Part B Eng 2016;99:305–11.
[37] Naddeo F, Naddeo A, Cappetti N. Novel “load adaptive algorithm based” procedure for 3D printing of cancellous bone-inspired structures. Compos Part B Eng 2017;115:60–9.
[38] Singh R, Singh R, Dureja JS, Farina I, Fabbrocino F. Investigations for dimensional accuracy of Al alloy/Al-MMC developed by combining stir casting and ABS replica based investment casting. Compos Part B Eng 2017;115:203–8.
[39] Amendola A, Nava EH, Goodall R, Todd I, Skelton RE, Fraternali F. On the additive manufacturing, post-tensioning and testing of bi-material tensegrity structures. Compos Struct 2015;131:66–71.
[40] Amendola A, Carpentieri G, de Oliveira M, Skelton RE, Fraternali F. Experimental investigation of the softening stiffening response of tensegrity prisms under compressive loading. Compos Struct 2014;117:234–43.
[41] Ngo D, Fraternali F, Daraio C. Highly nonlinear solitary wave propagation in Y-Shaped granular crystals with variable branch angles. Phys Rev E 2012;85.036602–1-10.
[42] Fraternali F, Marino A, Elsayed T, Della Cioppa A. On the structural shape optimization via variational methods and evolutionary algorithms. Mech Adv Mater Struct 2011;18:225–43.
[43] Fraternali F, Amendola A. Mechanical modeling of innovative metamaterials alternating pentamode lattices and confinement plates. J Mech Phys Solids 2017;99:259–71.
[44] Amendola A, Benzoni G, Fraternali F. Non-linear elastic response of layered structures, alternating pentamode lattices and confinement plates. Compos Part B Eng 2017;115:117–23.
[45] Amendola A, Smith CJ, Goodall R, Auricchio F, Feo L, Benzoni G, et al. Experimental response of additively manufactured metallic pentamode materials confined between stiffening plates. Compos Struct 2016;142:254–62.